Inorganic Chemistry

Article

pubs.acs.org/IC

Crystal Structure of $YbCu_6In_6$ and Mixed Valence Behavior of Yb in $YbCu_{6-x}In_{6+x}$ (x = 0, 1, and 2) Solid Solution

Udumula Subbarao and Sebastian C. Peter*

New Chemistry Unit, Jawaharlal Nehru Centre for Advanced Scientific Research, Jakkur, Bangalore, 560064, India

Supporting Information

ABSTRACT: High quality single crystals of $YbCu_6In_6$ have been grown using the flux method and characterized by means of single crystal X-ray diffraction data. $YbCu_6In_6$ crystallizes in the $CeMn_4Al_8$ structure type, tetragonal space group $I4/mmm$, and the lattice constants are $a = b = 9.2200(13)$ Å and $c = 5.3976(11)$ Å. The crystal structure of $YbCu_6In_6$ is composed of pseudo-Frank–Kasper cages filled with one ytterbium atom in each ring. The neighboring cages share corners along [100] and [010] to build the three-dimensional network. $YbCu_{6-x}In_{6+x}$ (x = 0, 1, and 2) solid solution compounds were obtained from high frequency induction heating and characterized using powder X-ray diffraction. The magnetic susceptibilities of $YbCu_{6-x}In_{6+x}$ (x = 0, 1, and 2) were investigated in the temperature range 2–300 K and showed Curie–Weiss law behavior above 50 K, and the experimentally measured magnetic moment indicates mixed valent ytterbium. A deviation in inverse susceptibility data at 200 K suggests a valence transition from Yb^{2+} to Yb^{3+} as the temperature decreases. An increase in doping of Cu at the Al2 position enhances the disorder in the system and enhancement in the trivalent nature of Yb. Electrical conductivity measurements show that all compounds are of a metallic nature.

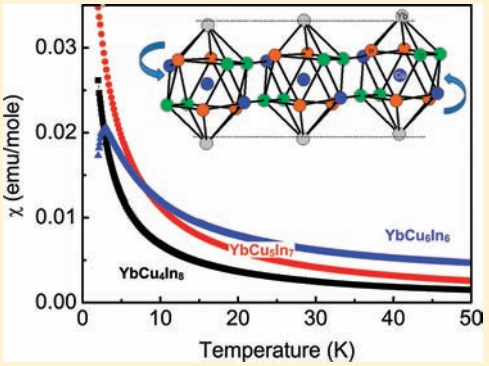

1. INTRODUCTION

The rare earth based intermetallic compounds of Ce, Eu, and Yb have attracted considerable attention in the past few decades because of their anomalous properties. These properties are associated with the valence instability of these rare earth ions. Recent studies have shown that the $RE_xT_yIn_z$ (RE = Ce, Eu, Yb, and T = transition metal) family of compounds can show interesting physical phenomena arising from competition associated with mixed valence effects. Some notable examples of mixed valence compounds are CeRhIn,[1] Ce_2RuZn_4,[2] $Yb_3AuGe_2In_3$,[3] $YbCu_4In$,[4] etc. Among the trivalent rare earth compounds, the Yb based intermetallics are considered as the counterparts to the isothermal cerium compounds (i.e., f^{13} vs f^1 systems) and have received considerable attention in the past few years. This interest originates from the ability of Yb to exhibit various peculiar properties such as intermediate valence, heavy fermions, Kondo behavior, unusual magnetism, and superconductivity.[5−9] These properties are generally believed to arise from the strong hybridization (interaction) between the localized 4f electrons and the delocalized s, p, and d conduction electrons.[10,11] One of the main motivations of the work described here is the continued development of the intermetallic chemistry of Yb[3,12−18] and a deeper understanding of the ability of Yb to adopt different or mixed oxidation states.

The Yb–Cu–In ternary system was investigated over the whole concentration range at 400 °C, and the isothermal section was reported by Kalychak et al.[19,20] So far, only a few compounds have been reported within the Yb–Cu–In system. The temperature dependent lattice constant for the $YbCu_4In$ compound was obtained by Kojima et al.[21] $YbCu_4In$ was essentially studied with respect to the Yb valence instability. This compound shows a first order temperature induced valence transition in the range 40–60 K from the Yb^{2+} nonmagnetic ground state to the Yb^{3+} magnetic high temperature state.[22−25] $Yb_{0.4}Cu_2In_{0.6}$ is another compound in this family which exhibits characteristic properties associated with a heavy-fermion system that was reported by Felner et al.[23,26]

$YbCu_{5.1}In_{6.9}$ was reported only for the powder X-ray diffraction (XRD),[27−29] crystallizing in the $CeMn_4Al_8$ type structure,[30,31] which is a modified structure of $ThMn_{12}$ type[32] with space group $I4/mmm$. Compounds of the $REFe_6Al_6$ (RE = rare earth)[33] and REM_4Al_8 (RE = rare earths, M = Cr, Mn, Fe, and Cu)[34] series crystallizing in the same structure type show interesting magnetic properties and hyperfine interactions. However, up to now, the physical properties of the $YbT_{6-x}In_{6+x}$ (T = transition metal) series have not been studied.

In this paper, we report the synthesis of $YbCu_6In_6$ using indium flux and the synthesis of solid solution $YbCu_{6-x}In_{6+x}$ (x = 0, 1, 2) using a high frequency (HF) induction heating method. We have studied the crystal structure of $YbCu_6In_6$ using single crystal X-ray diffraction. Magnetic susceptibility and electrical resistivity studies were performed on compounds obtained by high frequency induction heating. $YbCu_{6-x}In_{6+x}$ exhibits a magnetic transition that is associated with Yb^{2+} to

Received: March 14, 2012
Published: May 21, 2012

   dx.doi.org/10.1021/ic300552w | Inorg. Chem. 2012, 51, 6326–6332

Yb^{3+} valence change. A substantial difference in the magnetic moment and magnetic ordering upon different Cu/In doping was observed for these compounds. The mixed valence behavior of Yb in these compounds develops a disorder in the crystal structure associated with electron transfer and noticeable changes in the properties such as valence fluctuations and magnetic ordering.

2. EXPERIMENTAL SECTION

2.1. Reagents. The following reagents were used as purchased without further purification: Yb (ingots 99.99% Alfa-Aesar), Cu (ingots, 99.99% Alfa-Aesar), and In (shots, 99.99% Alfa-Aesar).

2.2. Synthesis. *2.2.1. Metal Flux Synthesis of $YbCu_6In_6$.* High quality single crystals of $YbCu_6In_6$ were obtained by combining 0.1 g of ytterbium, 0.408 g of copper, and 2.048 g of indium in an alumina (Al_2O_3) crucible under an inert gas atmosphere inside the glovebox. The crucible was placed in a 13 mm fused silica tube, which was flame-sealed under a vacuum of 10^{-3} Torr, to prevent oxidation during heating. The reactants were then heated to 1000 °C over 10 h and maintained at that temperature for 10 h to allow proper homogenization. The reaction was then cooled to 850 °C in 5 h and kept at this temperature for 96 h. Finally, the sample was allowed to slowly cool to 30 °C over 72 h. The reaction product was isolated from excess indium flux by heating at 450 °C and subsequently centrifuging through a coarse frit. Any remaining flux was removed by immersion and sonication in glacial acetic acid for 24 h. The final crystalline product was rinsed with water and dried with acetone. This method produced the target compound with ca. 99% purity and in a low yield on the basis of the initial amount of Yb metal used in the reaction. Small rod-shaped crystals of $YbCu_6In_6$ are carefully selected for elemental analysis and single crystal XRD data collection.

2.2.2. Synthesis of $YbCu_{6-x}In_{6+x}$ (x = 0, 1, 2) by High Frequency Induction Heating. Ytterbium, copper, and indium elements were mixed in the ideal 1:6:6, 1:5:7, and 1:4:8 atomic ratios and sealed in tantalum ampules under an argon atmosphere in an arc-melting apparatus. The tantalum ampules were subsequently placed in a water-cooled sample chamber of an induction furnace (Easy Heat induction heating system, Model 7590), first rapidly heated to 180 Amperes (850–950 °C) and kept at that temperature for 15 min. Finally, the reaction was rapidly cooled to room temperature by switching off the power supply. All compounds could easily be removed from the tantalum tubes. No reactions with the crucible material could be detected. All compounds were found to be stable in moist air for several days. They are in polycrystalline form and light gray in color. The weight losses of the final material were found to be less than 1%. The samples obtained from the high frequency induction heating method were used for the property studies.

2.3. Elemental Analysis. Semiquantitative microprobe analyses of the single crystals obtained from the flux techniques were performed with a scanning Leica 220i electron microscope (SEM) equipped with Bruker 129 eV energy dispersive X-ray analyzer (EDS). EDX analyses were done using P/B-ZAF standardless analysis. Data were acquired with an accelerating voltage of 20 kV and in 90 s of accumulation time. The EDS analysis performed on visibly clean surfaces of the single crystal obtained from the flux method indicated that the atomic composition was close to 1:6:6.

2.4. Powder X-Ray Diffraction. Phase identity and purity of the $YbCu_{6-x}In_{6+x}$ (x = 0, 1, 2) samples were determined by powder XRD experiments that were carried out with a Bruker D8 Discover diffractometer using Cu Kα radiation (λ = 1.54187 Å). The experimental powder patterns of $YbCu_{6-x}In_{6+x}$ (x = 0, 1, 2) were compared to the pattern calculated from the single-crystal X-ray structure refinement of the $YbCu_6In_6$ and were found to be in good agreement.

2.5. Single Crystal X-Ray Diffraction. A suitable single crystal of $YbCu_{6-x}In_{6+x}$ was mounted on a thin glass fiber with commercially available super glue. X-ray single crystal structural data of $YbCu_6In_6$ were collected on a Bruker X8 APEX II diffractometer equipped with a normal focus, a 2.4 kW sealed tube X-ray source with graphite monochromatic Mo Kα radiation (λ = 0.71073 Å) operating at 50 kV and 30 mA. The X-AREA (X-RED and X-SHAPE within) package suite[35] was used for the data extraction and integration and to apply numerical absorption corrections. The structure was solved by SHELXS 97 and refined by a full matrix least-squares method using SHELXL. Details of the crystallographic data are given in Tables 1–4.

Table 1. Crystal Data and Structure Refinement for $YbCu_{6.08}In_{5.92}$ at 296(2) K

empirical formula	$YbCu_{6.08}In_{5.92}$
fw	1239.13
temp	296(2) K
wavelength	0.71073 Å
cryst syst	tetragonal
space group	*I*4/*mmm*
unit cell dimensions	a = 9.2200(2) Å, α = 90.00°
	b = 9.2200(2) Å, β = 90.00°
	c = 5.3976(2) Å, γ = 90.00°
volume	458.84(2) $Å^3$
Z	2
density (calculated)	8.972 g/cm^3
absorption coeff	38.326 mm^{-1}
F(000)	1073
cryst size	0.1 × 0.06 × 0.06 mm^3
θ range for data collection	3.12 to 30.55°
index ranges	$-12 \le h \le 7$, $-13 \le k \le 13$, $-7 \le l \le 7$
reflns collected	2745
independent reflns	232 [R_{int} = 0.0476]
completeness to θ = 30.55°	100%
refinement method	full-matrix least-squares on F^2
data/restraints/params	232/0/17
goodness-of-fit	1.114
final R indices [$>2\sigma(I)$][a]	R_{obs} = 0.0415, wR_{obs} = 0.0998
extinction coefficient	0.0181(16)
largest diff. peak and hole	7.328 and −8.237 e·$Å^{-3}$

[a] $R = \sum ||F_o| - |F_c|| / \sum |F_o|$, $wR = \{\sum[w(|F_o|^2 - |F_c|^2)^2] / \sum[w(|F_o|^4)]\}^{1/2}$ and calcd $w = 1/[\sigma^2(F_o^2) + (0.0318P)^2 + 111.1197P]$ where $P = (F_o^2 + 2F_c^2)/3$.

Table 2. Atomic Coordinates (×10^4) and Equivalent Isotropic Displacement Parameters ($Å^2$ × 10^3) for $YbCu_{6.08}In_{5.92}$ at 296(2) K with Estimated Standard Deviations in Parentheses

label	Wyckoff site	x	y	z	occupancy	U_{eq}[a]
Yb	2*a*	0	0	0	1	3(1)
Cu	8*f*	2500	2500	2500	1	6(1)
In	8*i*	3398(2)	0	0	1	6(1)
M (Cu + In)	8*j*	2996(4)	5000	0	(0.52 + 0.48)	21(2)

[a] U_{eq} is defined as one-third of the trace of the orthogonalized U_{ij} tensor.

2.6. Magnetic Measurements. Magnetic measurements of $YbCu_{6-x}In_{6+x}$ (x = 0, 1, 2) were carried out on a Quantum Design MPMS-SQUID magnetometer. Measurements were performed on polycrystals, which were ground and screened by powder XRD to verify phase identity and purity. Temperature dependent data were collected for the field cooled mode (FC) between 2 and 300 K with an applied field of 1 kG. Magnetization data were also collected for $YbCu_{6-x}In_{6+x}$ (x = 0, 1, 2) at 2 and 300 K with field sweeping from −55 kOe to 55 kOe.

2.7. Electrical Resistivity. The resistivity measurements were performed in a 1 T field on the $YbCu_{6-x}In_{6+x}$ (x = 0, 1, 2) with a

dx.doi.org/10.1021/ic300552w | Inorg. Chem. 2012, 51, 6326–6332

Table 3. Anisotropic Displacement Parameters (Å² × 10³) for $YbCu_{6.08}In_{5.92}$ at 296(2) K with Estimated Standard Deviations in Parentheses[a]

label	U_{11}	U_{22}	U_{33}	U_{12}	U_{13}	U_{23}
Yb	3(1)	3(1)	3(1)	0	0	0
Cu	7(1)	7(1)	4(2)	1(1)	2(1)	2(1)
In	4(1)	5(1)	8(1)	0	0	0
M(Cu + In)	60(2)	2(2)	2(2)	0	0	0

[a]The anisotropic displacement factor exponent takes the form: $-2\pi^2[h^2a^{*2}U_{11} + ... + 2hka^*b^*U_{12}]$.

Table 4. Selected Bond Lengths [Å] for $YbCu_{6.08}In_{5.92}$ at 296(2) K with Estimated Standard Deviations in Parentheses

label	distances	label	distances
M−M	2.613(5)	In−In	2.954(3)
Cu−Cu	2.6988	In−M	2.9893(16)
Cu−M	2.7098(6)	Yb−In	3.1329(14)
In−Cu	2.7963(4)	Yb−M	3.2706(19)

conventional AC four probe setup. The samples were fabricated by pressing the powders into pellets applying 20 kN of pressure. These powder compacts, 0.2 mm in diameter and 0.5 mm in length, were pressed in a pellet die constructed in a manner which made it possible to press into the center of the pellet followed by annealing for 12 h at 333 K. The electrical contacts were made by colloidal silver paste and then annealed at approximately 353 K for 5 h. The data were collected in the range 3−300 K using a commercial Quantum Design Physical Property Measurement System (QD-PPMS). The results were reproducible for several batches.

3. RESULTS AND DISCUSSION

3.1. Reaction Chemistry. $YbCu_6In_6$ was obtained from the Yb−Cu−In reaction in liquid indium as a flux in high purity. The shiny gray-colored rod-shaped single crystals up to 1 mm in length were stable in the air, and no decomposition was observed even after several months. A typical SEM image of rod-like crystals of $YbCu_6In_6$ as grown from the flux synthesis is shown in Figure 1. After establishing the crystal structure of the

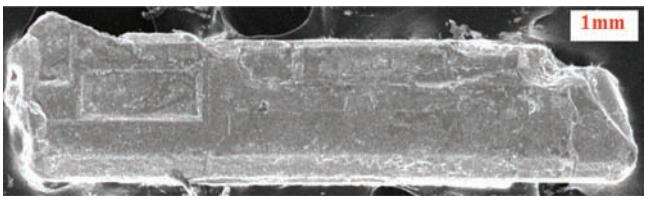

Figure 1. Typical SEM image of a $YbCu_6In_6$ single crystal grown from In flux.

compound, we have attempted to find the solubility range for $YbCu_{6-x}In_{6+x}$ and succeeded in the synthesis of $YbCu_6In_6$, $YbCu_5In_7$, and $YbCu_4In_8$ compounds using high frequency induction heating. These products form only as microcrystalline $YbCu_{6-x}In_{6+x}$ (x = 0, 1, 2) instead of large single crystals. Our attempt to synthesize a single phase of $YbCu_7In_5$ and $YbCu_3In_9$ was not successful. The XRD patterns of the powdered sample were recorded with a Bruker D8 advance X-ray diffractometer to confirm the phase purity of these compounds.

3.2. Structure Refinement of $YbCu_6In_6$. The atomic parameters of $YbCu_{5.9}In_{6.1}$[23] were taken as starting parameters, and the structure was refined using Shelxl-97 (full-matrix least-squares on F^2) with anisotropic atomic displacement parameters for all atoms. As a check for the correct composition, the occupancy parameters were refined in a separate series of least-squares cycles. Our data confirms the previously reported X-ray powder data,[26,27] but the atomic positions have been refined with higher precision. $YbCu_6In_6$ crystallizes in a body centered tetragonal lattice ($I4/mmm$) of the $CeMn_4Al_8$ type structure. There are four crystallographical positions in the $YbCu_6In_6$ structure: one ytterbium atom occupies 2*a* cerium site, while copper and indium atoms are distributed over the manganese and aluminum sites, 8*f*, 8*i*, and 8*j*. Initially, we attempted to refine the structure with one ytterbium, two copper, and one indium atom. During isotropic refinement of $YbCu_6In_6$, it was observed that the thermal parameters of the Cu atom at 8*j* were largely unsatisfactory, marked with relatively high residuals (R_1 > 15%) and large electron density residuals (30 e Å^{-3}) around copper atoms. The anomalous thermal parameters were not resolved by subsequent refinement of the occupancy parameters. Our attempts to substitute the Cu position with In also could not solve the large refinement values. All of these facts indicated a crystallographic disorder associated at the 8*j* position; consequently, Cu and In atoms were mixed and refined successfully with reasonably good thermal parameters but slightly large U_{11} and electron density residuals (~8 e Å^{-3}) probably due to a certain degree of disorder in $YbCu_6In_6$. This could be due to the strong distortions that happened because of the mixed position. The overall stoichiometry obtained from the refinement is $YbCu_{6.08}In_{5.92}$, rounded to the nearest integers as $YbCu_6In_6$.

The data collection and structure refinement for $YbCu_6In_6$ are listed in Table 1. The standard atomic positions and isotopic atomic displacement parameters of this compound are collected in Table 2. The anisotropic displacement parameters and important bond lengths are listed in Tables 3 and 4, respectively. Further information on the structure refinement is available from Fachinformationszentrum Karlsruhe, D-76344 Eggenstein-Leopoldshafen (Germany), by quoting the Registry No. CSD-424351.

3.3. Crystal Chemistry of $YbCu_6In_6$. The crystal structure of $YbCu_6In_6$ along the *c* axis is shown in Figure 2. $YbCu_6In_6$ crystallizes in the tetragonal $CeMn_4Al_8$ type structure (space group $I4/mmm$), which is an ordered superstructure of the $ThMn_{12}$ type. $YbCu_6In_6$ is slightly more distorted compared to the parent compound. An interesting feature of the $CeMn_4Al_8$

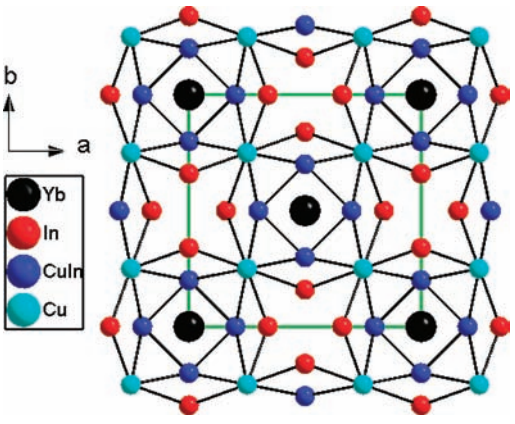

Figure 2. The structure of $YbCu_{6.08}In_{5.92}$ as viewed along the *c* axis. The unit cell is outlined as green solid lines.

dx.doi.org/10.1021/ic300552w | Inorg. Chem. 2012, 51, 6326−6332

compound is that Mn and Al atoms are not distributed at random over the three atomic positions available for these elements in the $ThMn_{12}$-type structure. By further substitution of Cu and In atoms in $YbCu_6In_6$, the Mn and Al2 positions, respectively, are completely occupied in the $CeMn_4Al_8$ structure, and the Al1 position is occupied with both Cu (52%) and In (48%) atoms (denoted as M). This mixed position could be one of the probable reasons for the enhanced distortions observed in the crystal structure of $YbCu_6In_6$. The Yb atoms occupy the 2*a* site of point symmetry (4/*mmm*). The Cu atom occupies the 8*f* site of point symmetry (2/*m*). The In atom occupies the 8*i* site of point symmetry (*m*2*m*) and 8*j* site occupied by mixture of Cu and In atoms of point symmetry (*m*2*m*). The crystal structure of $YbCu_6In_6$ is composed of pseudo Frank–Kasper cages $[Cu_8In_4M_8]$ filled with one ytterbium atom in each ring to form a stable structure. These pseudo-Frank–Kasper cages are shared through the corner M atoms along the *ab* plane, resulting in a three-dimensional network (Figure 3).

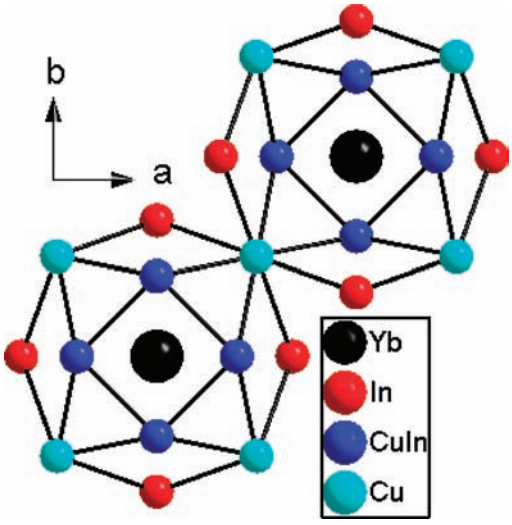

Figure 3. Pseudo-Frank–Kasper cages in $YbCu_6In_6$ shared through the corner M atoms along the *ab* plane.

The local coordination environments of Cu and In atoms within a radius of 3.6 Å are presented in Figures 4 and 5. The slight distortion of $YbCu_6In_6$ is clearly evident in the comparison of Mn ($CeMn_4Al_8$ structure) and Cu ($YbCu_6In_6$ structure) coordination environments (Figure 4), which in fact develop mixed valence behavior of the Yb atom in $YbCu_6In_6$. Considering the fact that Cu can exist as both monovalent and divalent, we assume a slight electron transfer from Cu to Yb will cause mixed valency at Yb, probably in the Cu atom as well, and enhanced Yb–Cu bond distances (3.528(1) Å) compared to the theoretical value. This is further confirmed in the magnetic measurements (discussed below) as the magnetic moments of Yb were enhanced upon adding more Cu atoms at the In position. The contribution of trivalent Yb is more in $YbCu_6In_6$ (88%) compared to the $YbCu_4In_8$ sample (13%). The coordination environment of In atoms is formed as a 14-vertex Frank–Kasper cage. M atoms are in the distorted icosahedron geometry composed of 12 atoms, of which two are Yb atoms and the remaining 10 atoms are shared by Cu and In atoms. All icosahedrons and Frank–Kasper cages are slightly distorted compared to the parent compounds.

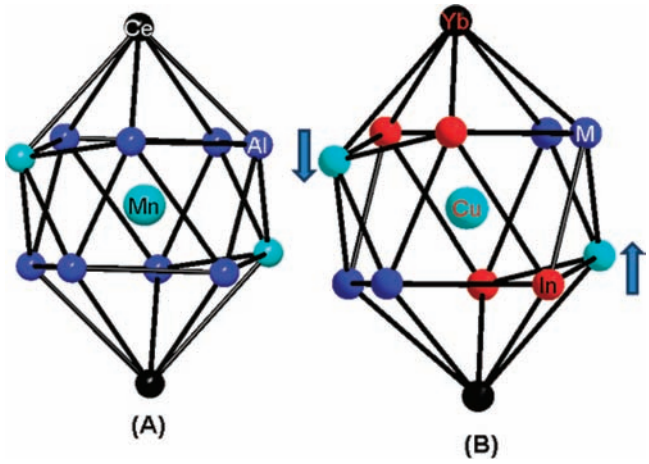

Figure 4. Comparison of the icosahedron polyhedra of Mn in $CeMn_4Al_8$ and Cu in $YbCu_{6-x}In_{6+x}$. The distortion at the Cu atom is marked as blue arrows.

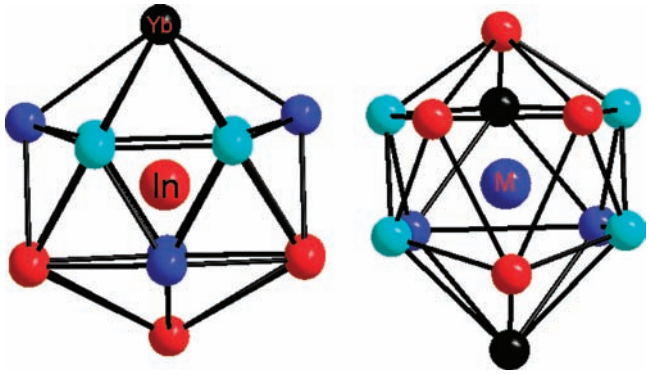

Figure 5. The coordination environment of In (A) and mixed atomic position (B) in $YbCu_{6.08}In_{5.92}$.

The M–M distance is the shortest bond distance (2.613(5) Å) in $YbCu_6In_6$, which is close to the atomic radii of the Cu–Cu distance (2.560 Å) observed in $YbCu_4Al_8$.[34] The shortest distance of Yb–In is 3.1329(14) Å smaller than the calculated distances of 3.38 Å[36] probably because of strong the covalent bond between the Yb and In atoms; however, the shortest distance between Yb and Cu atoms is 3.528(1) Å, substantially larger than the theoretical value of 3.22 Å,[36] suggesting a weak interaction between them. The Yb–M bond distance of 3.271(2) Å is lying between the Yb–Cu and Yb–In distances. The Cu sites along the *c* axis are connected with a bond distance of 2.6988(5) Å, which is a longer than the normal Cu–Cu distance, which is 2.560 Å, comparable in $Cu_2Y_{0.1}Yb_{0.3}In_{0.6}$,[26] $YbCuIn_4$,[37] etc. Yb–Cu bond distances of 3.5280(3) Å for Yb–Cu and 3.2707(5) Å for Yb–M are very close to the bond distance of $Yb–Cu^{+}$ (3.19 Å) compared to $Yb–Cu^{2+}$(3.06 Å), indicating that the copper atoms present in $YbCu_6In_6$ are in a monovalent nonmagnetic state.

3.4. Physical Properties. *3.4.1. Magnetism.* Magnetic susceptibility measurements were made on a polycrystalline sample of $YbCu_{6-x}In_{6+x}$ (x = 0, 1, 2) obtained from high frequency induction heating synthesis. The temperature dependent molar magnetic susceptibility (χ_m) and inverse susceptibility ($1/\chi_m$) of $YbCu_{6-x}In_{6+x}$ (x = 0, 1, 2) at an applied field of 1 kOe are shown in Figures 6 and 7, respectively. The susceptibility curve obeys modified Curie–Weiss law, $\chi = C/(T - \theta) + \chi_0$, above 50 in $YbCu_4In_8$ and $YbCu_5In_7$ and above 150

dx.doi.org/10.1021/ic300552w | *Inorg. Chem.* 2012, 51, 6326–6332

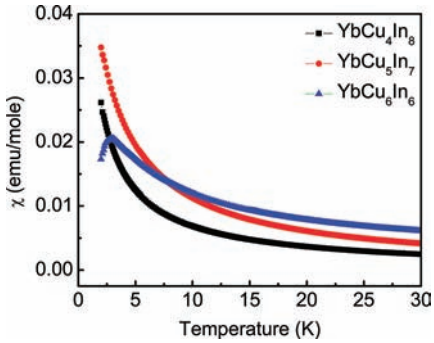

Figure 6. Temperature dependent magnetic susceptibility (χ_m) of $YbCu_4In_8$, $YbCu_5In_7$, and $YbCu_6In_6$.

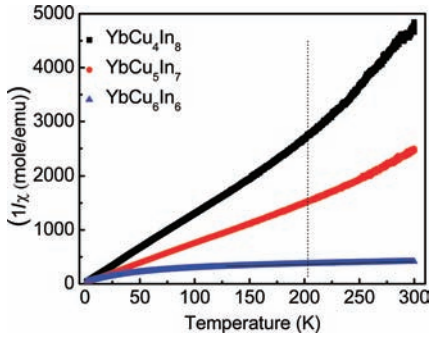

Figure 7. Temperature dependence of the modified reciprocal magnetic susceptibility ($1/\chi_m$) of the $YbCu_4In_8$, $YbCu_5In_7$, and $YbCu_6In_6$.

K in $YbCu_6In_6$. The magnetic susceptibility of $YbCu_6In_6$ shows a transition around 3 K. No magnetic ordering was observed in $YbCu_4In_8$ and $YbCu_5In_7$ compounds down to 2 K, but the susceptibility slightly increases at lower temperatures, which is normal for rare earth based intermetallics.[38]

In $YbCu_6In_6$, the susceptibility data begin to follow a modified Curie–Weiss law only in the temperature region above 150 K. At lower temperatures, the deviation can be attributed to crystal field contributions and/or to a possible onset of valence fluctuations. Above 150 K, $YbCu_6In_6$ exhibits paramagnetic behavior with an effective magnetic moment of 4.024 μ_B/Yb atom. The estimated experimental μ_{eff} value is about 88% of that expected for a free ion Yb^{3+} moment (4.56 μ_B/Yb).

However, the inverse magnetic susceptibility curves for $YbCu_4In_8$ and $YbCu_5In_7$ compounds are completely different from $YbCu_6In_6$ and present two linear regions in the temperature ranges 50–200 K and 200–300 K. The magnetic susceptibility in these two temperature ranges fits the modified Curie–Weiss law, and the effective magnetic moments obtained in the high temperature range region (200–300 K) are 0.61 and 0.9 μ_B/Yb for $YbCu_4In_8$ and $YbCu_5In_7$, respectively. These values are less than a quarter of the value expected for an Yb^{3+} ion. The calculated magnetic moment for Yb in $YbCu_4In_8$ (13% Yb^{2+}) is pretty close to the value observed for Yb in the $YbCr_4Al_8$ compound (10% Yb^{2+}).[34] This indicates that both compounds are in the same structure type, and assuming both Cu and Cr elements are nonmagnetic, the observed magnetic moments are due to the mixed valent nature of Yb atoms. A fit to the low temperature range (50–200 K) produced magnetic moments of 0.79 and 1.02 μ_B/Yb for $YbCu_4In_8$ and $YbCu_5In_7$, respectively, suggesting that these systems have a valence fluctuation of Yb^{2+} to Yb^{3+} below 200 K. It was observed that compounds crystallized in $CeMn_4Al_8$ type structures create disorder at the Mn and Al sites. Such disorders affect the magnetic behavior in the solid solution, and it was previously reported for $LaMn_{4+x}Al_8$.[39] In $YbCu_{6-x}In_{6+x}$ (x = 0, 1, 2), a small change in the Cu to In ratio reduces the magnetic moment substantially and valence fluctuations of the Yb atom. Assuming Cu and In are nonmagnetic elements in the systems,[40,41] this large difference in the magnetic moment could be associated with the structural behavior. Much more detailed structural studies such as neutron diffraction could give an insight to the structure–property relations in these compounds.

The field dependence of the magnetization $M(H)$ for ground samples of $YbCu_{6-x}In_{6+x}$ (x = 0, 1, 2) were measured at 2 and 300 K and can be seen in Figure 8. The data measured at 300 K

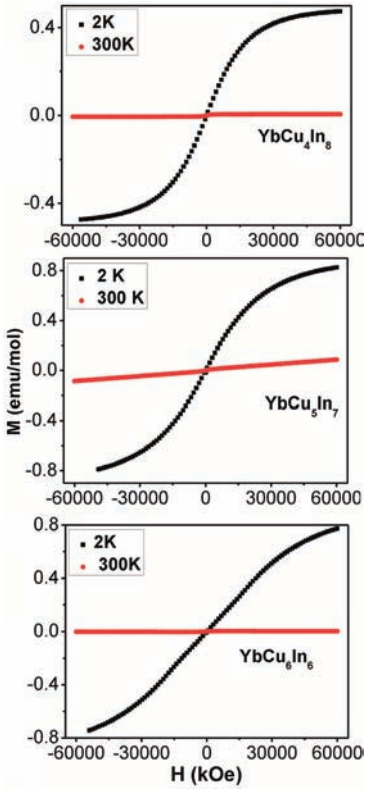

Figure 8. Magnetization as a function of applied magnetic field at 2 and 300 K for a polycrystalline sample of $YbCu_4In_8$, $YbCu_5In_7$, and $YbCu_6In_6$.

exhibit linear behavior, and no signs of saturation up to our highest attainable field of 60 kG. The magnetization curve taken at 2 K (within the magnetic ordering) shows a slight field dependent response up to ~30 kOe and continues to rise slowly up to the highest obtainable field (60 kG). However, the saturation behavior is different for each system at the highest field. The $YbCu_4In_8$ system almost saturates at ~30 kOe with a magnetic moment of ~0.5 emu/mol. $YbCu_5In_7$ saturates at a high value with higher saturation magnetic moments, and $YbCu_6In_6$ does not saturate even at the highest applied magnetic field.

3.4.2. Electrical Resistivity. The normal state temperature dependent resistivity of $YbCu_{6-x}In_{6+x}$ (x = 0, 1, 2) is shown in Figure 9. This continuously decreases linearly with decreasing

dx.doi.org/10.1021/ic300552w | Inorg. Chem. 2012, 51, 6326–6332

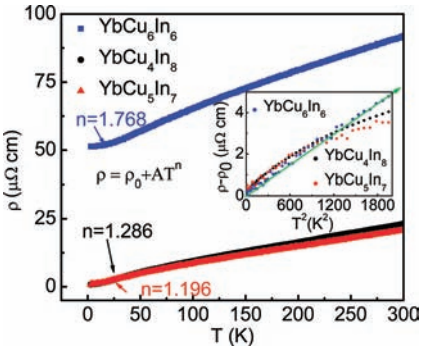

Figure 9. Resistivity (ρ) measured as a function of the temperature. The low temperature data have been fitted to the power law, $\rho = \rho_0 + AT^n$. The values obtained from the fit are shown in the figure.

temperature, typical for metallic systems[42,43] but without any long-range magnetic ordering. The resistivity values of $YbCu_4In_8$, $YbCu_5In_7$, and $YbCu_6In_6$ are 24 $\mu\Omega$ cm, 22 $\mu\Omega$, and 92 $\mu\Omega$, respectively, at room temperature.

At low temperatures in the range of 0−50 K, the $\rho(T)$ data can be fitted to the power law function, $\rho = \rho_0 + AT^n$, where ρ_0 is the residual resistivity expressed in units of Ω cm and A and n are the fitting parameters. The values obtained from the fit are shown in Figure 9. According to Fermi-liquid theory, at low temperatures, the resistivity varies as $\rho = \rho_0 + AT^2$. Experimentally, it has been observed that when electron−electron scattering dominates over electron−phonon scattering, $\rho \propto T^2$. The value obtained from the fit power is close to 2 in $YbCu_6In_6$, which is the case for systems exhibiting a Fermi liquid state.[44,45] But in $YbCu_4In_8$ and $YbCu_5In_7$, the value obtained from the fit power is 1.28 and 1.19, respectively, characteristic for a non-Fermi liquid state.[46] In order to verify Fermi liquid and non-Fermi liquid behavior, the resistivity data are plotted as $(\rho - \rho_0)$ vs T^2 as an inset to Figure 9. For $YbCu_6In_6$, linearity in the data confirms Fermi-liquid behavior in this compound at low temperatures, while the other two compounds show a deviation in the curve.

4. CONCLUDING REMARKS

High quality single crystals of $YbCu_6In_6$ were obtained from the metal flux technique, and the crystal structure of $YbCu_6In_6$ was studied using single crystal X-ray diffraction. The solid solution, $YbCu_{6-x}In_{6+x}$ (x = 0, 1 and 2), obtained from the high frequency induction heating treatment was studied by X-ray powder diffraction methods. The magnetic susceptibility of $YbCu_6In_6$ followed modified Curie−Weiss law in the temperature range of 155 to 300 K, with an effective magnetic moment of 4.024 μ_B/Yb atom. The estimated experimental μ_{eff} value is 88% of Yb^{3+} compared to the theoretical value of 4.56. A significant difference in the magnetic moment of $YbCu_4In_8$ and $YbCu_5In_7$ could be associated with strong structural disorder in these systems, and a change in the linearity in modified inverse magnetic susceptibility curves suggests a valence transition from the diamagnetic Yb^{2+} state to Yb^{3+}. The physical properties of $YbCu_{6-x}In_{6+x}$ (x = 0, 1, and 2) exhibit that there exists a Fermi-liquid regime at low temperature as $\rho \propto T^2$. Systematic temperature and magnetic field dependent structural and physical property measurements on these compounds will bring out interesting physical phenomena.

■ ASSOCIATED CONTENT

Supporting Information

Crystallographic information files (CIF). This material is available free of charge via the Internet at http://pubs.acs.org.

■ AUTHOR INFORMATION

Corresponding Author

*Phone: 080-22082298. Fax: 080-22082627. E-mail: sebastiancp@jncasr.ac.in.

Notes

The authors declare no competing financial interest.

■ ACKNOWLEDGMENTS

We thank JNCASR and Department of Science and Technology, Government of India for financial support. U.S. thanks CSIR for a research fellowship, and S.C.P thanks the Ramanujan Fellowship from the Department of Science and Technology, Government of India. The authors thank Rana, Bharat, Sreenivas, Mahesh, and Kishore for various measurements.

■ REFERENCES

(1) Adroja, D. T.; Malik, S. K.; Padalia, B. D.; Vijayaraghavan, R. *Phys. Rev. B* **1989**, *39*, 4831−4833.
(2) Mishra, R.; Hermes, W.; Rodewald, U. C.; Hoffmann, R.-D.; Pöttgen, R. *Z. Anorg. Allg. Chem.* **2008**, *634*, 470−474.
(3) Chondroudi, M.; Peter, S. C.; Malliakas, C. D.; Balasubramanian, M.; Li, Q. A.; Kanatzidis, M. G. *Inorg. Chem.* **2011**, *50*, 1184−1193.
(4) Nowik, I.; Felner, I.; Voiron, J.; Beille, J.; Najib, A.; Lachiesserie, E. d. T. d.; Gratz, E. *Phys. Rev. B* **1988**, *37*, 5633−5638.
(5) Kindler, B.; Finsterbusch, D.; Graf, R.; Ritter, F. *Phys. Rev. B* **1994**, *50*, 704−707.
(6) Bauer, E. *Adv. Phys.* **1991**, *40*, 417−534.
(7) Wachter, P. *Handbook on the Physics and Chemistry of Rare Earths*; Gschneidner, K. A., Jr., Eyring, L., Lander, G. H., Chappin, G. R., Eds.; Elsevier: Amsterdam, 1994; Vol. 19, p 177.
(8) Braun, H. F.; Segre, C. U. *Solid State Commun.* **1980**, *35*, 735−738.
(9) Hausermannberg, L. S.; Shelton, R. N. *Phys. Rev. B: Condens. Matter* **1987**, *35*, 6659−6664.
(10) Lawrence, J. M.; Riseborough, P. S.; Park, R. D.; Prog, R. *Phys. Rev. B* **1981**, *44*, 1−84.
(11) Fisk, Z.; Hess, D. W.; Pethick, C. J.; Pines, D.; Smith, J. L.; Thomson, J. D.; Willis, J. O. *Science* **1988**, *239*, 33−42.
(12) Chondroudi, M.; Balasubramanian, M.; Welp, U.; Kwok, W. K.; Kanatzidis, M. G. *Chem. Mater.* **2007**, *19*, 4769−4775.
(13) Zhuravleva, M. A.; Kanatzidis, M. G. *J. Solid State Chem.* **2003**, *173*, 280−292.
(14) Zhuravleva, M. A.; Salvador, J.; Bilc, D.; Mahanti, S. D.; Ireland, J.; Kannewurf, C. R.; Kanatzidis, M. G. *Chem.—Eur. J.* **2004**, *10*, 3197−3208.
(15) Sebastian, C. P.; Salvador, J.; Martin, J. B.; Kanatzidis, M. G. *Inorg. Chem.* **2010**, *49*, 10468−10474.
(16) Sebastian, C. P.; Kanatzidis, M. G. *J. Solid State Chem.* **2010**, *183*, 2077−2081.
(17) Margadonna, S.; Prassides, K.; Chondroudi, M.; Salvador, J. R.; Kanatzidis, M. G. *Chem. Commun.* **2005**, *46*, 5754−5756.
(18) Wu, X. N.; Francisco, M.; Rak, Z.; Bakas, T.; Mahanti, S. D.; Kanatzidis, M. G. *J. Solid State Chem.* **2008**, *181*, 3269−3277.
(19) Kalychak, Y. M. *Russ. Metall.* **1998**, *4*, 138−148.
(20) Kalychak, Y. M.; Zaremba, V. I.; Pöttgen, R.; Lukachuk, M.; Hoffmann, R. *Cryst. Struct., Phys. Prop., Phase Relat., Phase Diagram, Rev., 402* **2005**, *34*, 1−133.
(21) Kojima, K.; Nakai, Y.; Suzuki, T.; Asano, H.; Izumi, F.; Fujita, T.; Hihara, T. *J. Phys. Soc. Jpn.* **1990**, *59*, 792−795.
(22) Felner, I.; Nowik, I. *Phys. Rev. B* **1986**, *33*, 617−619.

(23) Felner, I.; Nowik, I.; Vaknin, D.; Potzel, U.; Moser, J.; Kalvius, G, M.; Wortmann, G.; Schmiester, G.; Hilscher, G.; Gratz, E.; Schmitzer, C.; Pillmayr, N.; Prasad, K. G.; De Waard, H.; Pinto, H. *Phys. Rev. B* **1987**, *35*, 6956−6963.
(24) Severing, A.; Gratz, E.; Rainford, B. D.; Yoshimura, K *Physica B* **1990**, *163*, 409−411.
(25) Kojima, K.; Hayashi, H.; Minami, A.; Kasamatsu, Y.; Hihara, T. *J. Magn. Magn. Mater.* **1989**, *81*, 267−272.
(26) Felner, I.; Nowik, I. *J. Magn. Magn. Mater.* **1987**, *63*−*64*, 615−617.
(27) Suski, W.; Wochowski, K.; Bodak, O. I.; Kalychak, Y. M.; Zaremba, V. I.; Mydlarz, T. *J. Alloys Compd.* **1997**, *250*, 642−645.
(28) Sysa, L. V.; Kal'ichak, Y. M.; Akhmad, B.; Baranyak, V. M. *Sov. Phys. Crystallogr.* **1989**, *34*, 443−444.
(29) Zaved, I. V. U. *Tsvetn. Metall.* **1990**, 1−99.
(30) Buschow, K. H. J.; Van Vucht, J. H. H.; Van Den Haagenhof, W. W. *J. Less-Common Met.* **1976**, *50*, 145−150.
(31) Zarechnyuk, O. S.; Krypyakevych, P. I. *Sov. Phys. Crystallogr.* **1962**, *7*, 436−446.
(32) Florio, J. V.; Rundle, R. E.; Snow, A. I. *Acta Crystallogr.* **1952**, *5*, 449−457.
(33) Felner, I.; She, M.; Rakavy, M.; Nowik, I. *J. Phys. Chem. Solids* **1981**, *42*, 369−377.
(34) Felner, I.; Nowik, I. *J. Phys. Chem. Solids* **1979**, *40*, 1035−1044.
(35) *X-Area*; Stoe, GmbH: Darmstadt, Germany, 2006.
(36) Donohue, J. *The Structures of the Elements*; Wiley: New York, 1974.
(37) Adroja, D. T.; Malik, S. K.; Padalia, B. D.; Vijayaraghavan, P. R. *J. Phys. C: Solid State Phys.* **1987**, *20*, L307−L310.39.
(38) Peter, S. C.; Rayaprol, S.; Francisco, M. C.; Kanatzidis, M. G. *Eur. J. Inorg. Chem.* **2011**, 3963−3968.
(39) Yamasaki, T.; Matsui, K.; Nakamura, H.; Shiga, M. *Solid State Commun.* **2001**, *119*, 415−418.
(40) Chełmicki, L.; Leciejewicz, J.; Zygmunt, A. *J. Phys. Chem. Solids* **1985**, *46*, 529−538.
(41) Bauer, E.; Hauser, R.; Gratz, E.; Gignow, D.; Schmitt, D.; Serenis, J. *J. Phys. Chem. Solids* **1992**, *4*, 7829−7838.
(42) He, J.; Ling, G.; Jiao, Z. *Physica B* **2001**, *301*, 196−202.
(43) Dremoa, R. V.; Koblyuk, N.; Mudryk, Y.; Romak, L.; Sechovsk, V. *J. Alloys Compd.* **2001**, *317*−*318*, 293−296.
(44) Varma, C. M. *Rev. Mod. Phys.* **1976**, *48*, 219−238.
(45) Peter, S. C.; Malliakas, C. D.; Nakotte, H.; Kothapilli, K.; Rayaprol, S.; Schultz, A. J.; Kanatzidis, M. G. *J. Solid State Chem.* **2012**, *187*, 200−207.
(46) Maple, M. B.; Seaman, C. L.; Gajewski, D. A.; Dalichaouch, Y.; Barbetta, V. B.; Andrade, M. C. d.; Mook, H. A.; Lukefahr, H. G.; Bernal, O. O.; Maclaughlin, D. E. *J. Low Temp. Phys.* **1994**, *95*, 1−2.